ISBN: 978-3-95450-179-3 doi:10.18429/JACoW-FEL2017-TUP004

LONGITUDINAL PHASE SPACE OPTIMIZATION FOR THE HARD X-RAY SELF-SEEDING

S. Liu†, W. Decking, G. Feng, V. Kocharyan, I. Zagorodnov, DESY, Hamburg, Germany
G. Geloni, S. Serkez, European XFEL, Schenefeld, Germany

Abstract

For the implementation of Hard X-Ray Self-Seeding (HXRSS) at European XFEL, short electron bunches (FWHM ≤ 50 fs) are preferred to mitigate spatio-temperal coupling effect and to fit to the seeding bump width. Therefore, operations with low charges (< 250 pC) are of interest. Longitudinal phase space optimization has been performed for the 100 pC case by flattening the current distribution. Start-to-end simulations show that, with the optimized distribution, for the photon energy of 14.4 keV, the HXRSS output power, pulse energy and spectral intensity can be increased by a factor of two compared to the nominal working point.

INTRODUCTION

The European XFEL [1] is driven by a superconductive linear accelerator operated with three bunch compressors (see Fig. 1 top) to enable operation with high peak current (~ 5 kA) and low transverse emittance at different charges (20 pC – 1 nC). Since the injector laser pulse length is the same for all the charges, the smaller the charge is, the larger compression is required to keep the same peak current. Different compression scenarios have been studied for the European XFEL to maximize the RF tolerances and minimize collective effects [2-4].

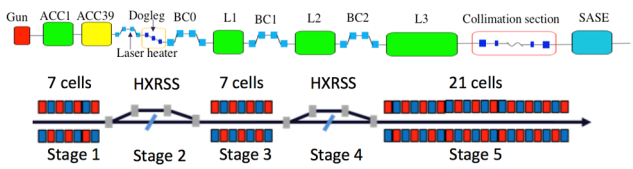

Figure 1: Schematic layout of European XFEL beam line (top) and HXRSS in SASE2 (bottom).

Hard X-ray Self-Seeding (HXRSS) is a well-known scheme to increase the X-ray longitudinal coherence and brightness simultaneously [5]. It has been successfully demonstrated at LCLS in 2012 [6]. The HXRSS at the European XFEL is planned to be implemented in the SASE2 beam line in 2018 (see Fig.1 bottom) [7, 8]. For the implementation of HXRSS at European XFEL, short electron beam bunches (FWHM ≤ 50 fs) are preferred to mitigate spatio-temperal coupling effect [9] and to fit to the seeding bump width. HXRSS simulations have been performed for several cases with different electron beam charges (100 pC and 250 pC) and output photon energies (9 keV-14.4 keV) [10, 11]. In these simulations, the input electron beam distributions used were, however, not fully optimized for self-seeding.

† shan.liu@desy.de

One example of the current profile and longitudinal phase space obtained from start to end (S2E) simulation is shown in Fig. 3 (top right, before undulator) for the 100 pC case with the nominal compression parameters. One can see a relatively narrow spike (FWHM≈12 fs) with a peak current of ~ 5 kA. This spike is much more pronounced for lower charges than for higher charges due to the larger compression. Due to this spike, the lower charges suffer more from CSR effects in the bunch compressors, especially in BC2 and in the collimation section, which causes a nonlinear energy distribution along the bunch. The nonlinearity in the longitudinal phase space can seriously deteriorate the HXRSS performance. It results in multi-peaks in the final output power (if tapering is not applied) and in the spreading in photon spectrum. Thus, for the HXRSS, it is preferable to have a "flat top" current distribution, which mitigates the CSR energy loss in the bunch compressors and avoids long head or tails to obtain both higher spectral intensity and pulse energy. In the following sections, we present the study of the longitudinal phase space optimization for the 100-pC case with beam dynamics simulations including HXRSS.

OPTIMIZATION PROCEDURES

At the European XFEL, a third harmonic RF cavity ACC39, which is installed in the injector right after the booster cavity ACC1 (see Fig.1, top), is used to linearize the energy profile and to control the shape of the current profile. The combination of RF parameters of ACC1 and ACC39 defines the 1st derivative p' (chirp), the 2nd derivative p'' (curvature) and the 3rd derivative p''' (skewness) of the momentum p before the first bunch compressor BC0 as follows [3]:

$$\begin{bmatrix} 1 & 0 & 1 & 0 \\ 0 & -k & 0 & -(nk) \\ -k^2 & 0 & -(nk)^2 & 0 \\ 0 & k^3 & 0 & (nk)^3 \end{bmatrix} \bullet \begin{bmatrix} V_{1,1}\cos\phi_{1,1} \\ V_{1,1}\sin\phi_{1,1} \\ V_{1,3}\cos\phi_{1,3} \\ V_{1,3}\sin\phi_{1,3} \end{bmatrix} = \begin{bmatrix} 1 \\ p_0^{'(1)} \\ p_0^{''(1)} \\ p_0^{'''(1)} \end{bmatrix} \quad (1)$$

where k is the wave number of the fundamental RF, n is the harmonic number (in our case, n=3), $V_{1,1}$, $V_{1,3}$, $\phi_{1,1}$, $\phi_{1,3}$ are the voltage amplitude and phase of fundamental and third harmonic RF, respectively.

The parameter that plays the main role in our optimization is the skewness p''', since it changes the ratio of compression in different parts of the bunch (i.e. the flatness). After changing p''', one can adjust the curvature p'' to control the symmetry of the current distribution. Since the goal is to add more compression to the head and tail particles. In the new configuration, we significantly decreased the 3rd derivative p''' from -226.3 to -5.05x10^4,

ISBN: 978-3-95450-179-3 doi:10.18429/JACoW-FEL2017-TUP004

and the 2nd derivative p'' is changed from 463.05 to 437.06. Figure 2 (top-left) shows the resulting RF sum voltage of A1 and AH1 in comparison with the nominal configuration. In the zoomed plot (Fig. 2 bottom-left), one can see that, the chirp in the center is not changed, however, in the head and tail region, the chirp is increased. This means that the head and tail particles can be compressed more forming a "flat top" current profile.

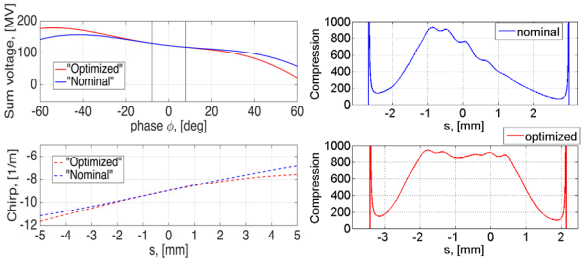

Figure 2: Left: sum voltage of ACC1 and ACC39 (top), the black lines indicate the edge of the bunch and this region is zoomed in (bottom) showing the energy chirp; Right: compression factor along the bunch for the nominal (blue) and the optimized (red) configuration.

The optimized RF parameters are shown in Table 1. Since the compression factor (C) at each stage has been optimized in the design to maximize the RF tolerance [4], in our optimization, we kept the chirp and R56 at the first stage unchanged and modified only slightly the chirp at stage 2 and stage 3 to obtain ~5 kA peak current. The simulation procedure and codes used are the same as presented in Ref. [12]. RF tweak 5 [13] is used for the calculation of RF parameters, which are taken as the initial input for the S2E simulations. A total number of 10^6 particles have been used in the simulation. Several iterations have been performed and the RF parameters have been adjusted at each iteration until we get the "flat top" current profile with ~5 kA peak current. Figure 2 (right) shows the global compression along the bunch with the nominal and optimized configurations calculated from S2E simulation. Once can see that, in both cases, a maximum compression factor of ~870 is achieved. However, in the optimized case, the compression is more flat in the bunch center. Similar optimizations have been performed before, for the energy dechirper studies with 250 pC and 500 pC charges [14]. In the next section, we present the optimization results for 100 pC and the HXRSS simulations with the optimized beam profile.

Table 1: The RF Parameters for the Nominal and the Optimized Configurations

	$V_{1,1}$ MV	$\phi_{1,1}$ deg	$V_{1,3}$ MV	$\phi_{1,3}$ deg	P' m^{-1}	P'' m^{-2}	P''' m^{-3}
Nominal	156.7	18.0	25.6	184.1	-8.98	463.05	-226.3
Optimized	173.1	30.9	29.3	211.5	-8.98	437.06	-5.05e4
	V_2 MV	ϕ_2 deg	P_2' m^{-1}	V_3 MV	ϕ_3 deg	P_3' m^{-1}	V_4 MV
Nominal	639.6	27.2	-11.4	1.832e3	21.5	-7.6	1.51e4
Optimized	641.7	27.6	-11.6	1.832e3	21.5	-7.6	1.51e4

OPTIMIZATION RESULTS

Figure 3 shows the comparison of the current distribution and the longitudinal phase space before and after the optimization. Since the main parameter change is in the injector, one can already see the difference in the current profile after BC0. Due to more compression on the head particles, in the optimized case, the current distribution is asymmetric with respect to the reference particle position (at 0 mm) after BC0. However, later on, due to the space charge effect in the linac L1, the distribution becomes more symmetric and more flat after BC1. After BC2, one can see a significant improvement in the compression of the head and the tail particles (4% of the head and tail particles, which are in the over compressed region, are excluded from the particle distributions after BC2 and before the undulator).

Comparing with the nominal profile, the optimized one is more flat in the top and the current FWHM increased from 12 fs to 15 fs. Meanwhile, the distortion in phase space is less pronounced after optimization. However,

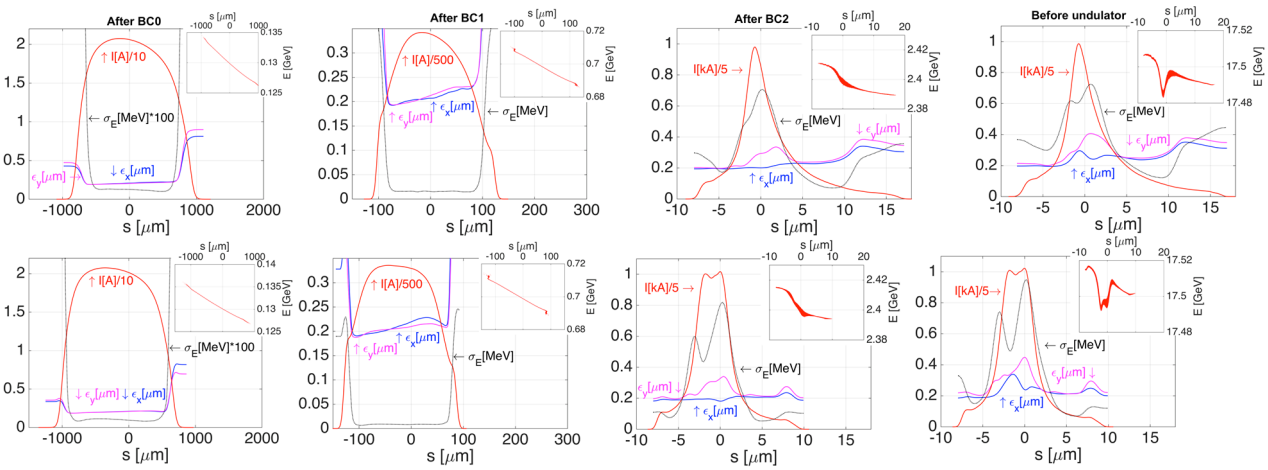

Figure 3: Current distribution, slice emittance and energy spread with longitudinal phase space (up-right plot in each subplot) for 100 pC before (top) and after (bottom) optimization. From left to right: after BC0, BC1, BC2 and before undulator.

ISBN: 978-3-95450-179-3 doi:10.18429/JACoW-FEL2017-TUP004

since the chirp in the head and the tail is larger than in the beam center (see Fig. 2), a small double-horn structure is formed in the current distribution after BC2 (more tuning in the skewness is required to get rid of the double-horn). The double-horn structure continues to affect the longitudinal phase space, and due to space charge effect in L3 and CSR effect in the collimation section, the longitudinal phase space ended up with a double-valley structure (see Fig. 3, before undulator). However, both the double-horn and the double-valley are not very pronounced and can not affect the HXRSS performance according to the following HXRSS simulations.

HXRSS SIMULATIONS

HXRSS simulations have been performed using OCELOT [15] which relies on GENESIS [16] for SASE calculations. The spatio-temperal coupling effect is included in the simulations. The input beam distributions used are from the S2E simulation as presented in Fig. 3 (before undulator). The simulation is divided into 5 stages, the HXRSS system is located at 2nd and 4th stage (8th and the 16th undulator section) and the other stages are undulator beam lines (see Fig. 1, bottom). Simulations have been performed with the crystal surface C400 for the 14.4 keV photon energy (highest energy of interest for HXRSS).

Figure 4 shows the simulation results for the "nominal" and the "optimized" distributions with and without uniform tapering of the undulator parameter K at stages 3 and 5. Uniform tapering is applied to compensate the large energy losses upstream. Without uniform tapering, the lasing in the peak current slices would be supressed due to large energy loss and lasing at the neighbouring slices would be enlarged due to smaller energy losses. The K value is therefore scanned for the "nominal" and "optimized" cases separately, and the optimal K is chosen to get maximum pulse energy and spectral density at the end of stage 5. At stage 5, the simulation is performed up to 12 undulator sections (5-m long segments with 1.1-m intersections).

The increment of pulse energy along stage 5 is shown in Fig. 4 (top-left). The reference point for HXRSS performance comparison is taken at the saturation point of the pulse energy (after ~ 9 undulators). The energy and energy spread distribution at the saturation point are shown in Fig. 4 (top-right). As mentioned before, the valley in the phase space, formed by collective effects, became more flat for both the "nominal" and "optimized" configurations after lasing. However, the "optimized" distribution lases in a wider range longitudinally than the "nominal" case since the FWHM of current distribution is larger and the valley in energy distribution is also wider. The radiation power is also higher for "flat top" as shown in Fig. 4 (bottom-left). One can also see that by applying the uniform tapering in stage 3 and stage 5, the radiation power increases of about factor 2 in both cases. Meanwhile, as shown in Fig. 4 (bottom-right), the spectral intensity also increased by factor 2 for the "optimized" case after uniform tapering. However, in the "nominal" case, the spectral density didn't increase significantly and a second peak appeared due to the lasing amplified in the region with slightly different energy and smaller energy spread (on the two sides of the peak current).

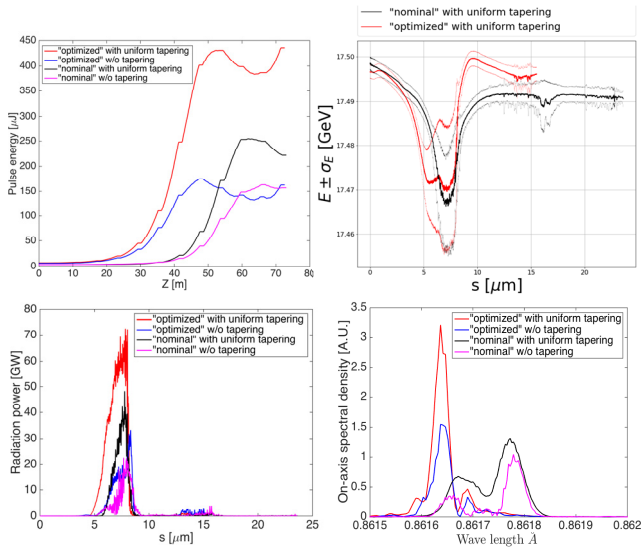

Figure 4: Top-left: pulse energy along the undulator beam line (at stage 5 with 12 undulators); top-right: energy and energy spread distribution at saturation (after 9 undulators); radiation power (bottom-left) and on-axis spectral density (bottom-right) at saturation for the "nominal" and the "optimized" cases with and w/o uniform taper.

SUMMARY AND DISCUSSIONS

We have performed longitudinal phase space optimization for the 100-pC case for the HXRSS application. We added more compression to the head and tail particles by significantly decreasing the 3rd derivative of momentum after the third harmonic RF cavity, which flattened the current distribution. S2E simulations have been performed taking into account the collective effects. The FWHM of current distribution is increased from 12 fs to 15 fs and the total bunch length is decreased from 80 fs to 60 fs. With the flattening of the peak current, the valley in the longitudinal phase space formed by the collective effects also gets wider. By applying a uniform tapering in stage 3 and stage 5 in the HXRSS simulations, the pulse energy, peak power and the spectral density have been increased by factor 2 at the saturation point. Further increase of power and spectral density is expected by applying tapering to the rest of the undulator beam line (12 undulators in our case).

The optimized distribution is particularly interesting for higher photon energy operation (e.g. 14.4 keV), since the higher the photon energy, the longer gain length is required to obtain the seed power required. However, since the RF tolerance for 100 pC operations is much higher than for higher charges [17], an experimental demonstration and stability study for the optimized setup is essential, and will be the subject of further investigations.

ACKNOWLEDGEMENTS

The authors would like to thank B. Beutner, M. Dohlus, M. Scholz and T. Limberg for helpful discussions.

ISBN: 978-3-95450-179-3 doi:10.18429/JACoW-FEL2017-TUP004

REFERENCES

[1] M. Altarelli *et al.*, "XFEL: The European X-Ray Free-Electron laser technical design report", DESY, Hamburg, Germany, DESY 2006-097, 2006.

[2] G. Feng *et al.* "Beam Dynamics Simulations for European XFEL", DESY, Hamburg, Germany, TESLA-FEL Report 2013-04, 2013.

[3] M. Dohlus and T. Limberg, *Proc. IPAC'05*, SLAC, Stanford, p. 250.

[4] I. Zagorodnov and M. Dohlus, "Semianalytical modeling of multistage bunch compression with collective effects", *PRST-AB*, vol. 14.1, p. 014403, 2011.

[5] G. Geloni, V. Kocharyan and E. Saldin, "A novel self-seeding scheme for hard X-ray FELs", *Journal of Modern Optics*, 58(16), pp.1391-1403, 2011.

[6] J. Amann *et al.*, "Demonstration of self-seeding in a hard-X-ray free-electron laser", *Nature Photonics*, 6 (10), pp. 693-698, 2012.

[7] G. Geloni, V. Kocharyan and E. Saldin, "A Cascade self-seeding scheme with wake monochromator for narrow-bandwidth X-ray FELs", DESY, Hamburg, Germany, DESY 10-080, June 2010.

[8] X. Dong *et al.,* "Status of the Hard X-ray Self-seeding project at the European XFEL", presented at FEL'17, MOP008.

[9] R. R. Lindberg and Y. V. Shvyd'ko, "Time dependence of Bragg forward scattering and self-seeding of hard x-ray free-electron lasers", *PRST-AB,* vol. 15(5), p. 050706, 2012.

[10] G. Geloni, V. Kocharyan and E. Saldin, "Scheme to increase the output average spectral flux of the European XFEL at 14.4 keV", DESY, Hamburg, Germany, DESY 15-141, August 2015.

[11] O. Chubar *et al.*, "Ultra-high-resolution inelastic X-ray scattering at high-repetition-rate self-seeded X-ray free-electron lasers", *Journal of Synchrotron Radiation*, vol. 23.2, pp. 410-424, 2016.

[12] I. Zagorodnov, G. Feng and T. Limberg, "Corrugated structure insertion for extending the SASE bandwidth up to 3% at the European XFEL", *Nucl. Instr. Meth. A*, vol. 837, pp. 69-79, 2016.

[13] B. Beutner, "RF Tweak 5 Tool for FLASH and XFEL. RF Tweak 5 Tool for FLASH and XFEL", FEL Seminar, DESY, Hamburg, Germany, Feb. 2015.

[14] G. Feng, "Beam Energy Dechirping Study for EXFEL", Beam Dynamics Group Meeting, DESY, Hamburg, Germany, Nov. 2015, http://www.desy.de/fel-beam/s2e/talks/2015_11_16/feng.pdf

[15] I. Agapov *et al.,* "OCELOT: A software framework for synchrotron light source and FEL studies", *Nucl. Instr. Meth. A*, vol. 768, pp. 151-156, 2014.

[16] G. Reiche, "GENESIS 1.3: a fully 3D time-dependent FEL simulation code", *Nucl. Instr. Meth. A*, vol. 429.1, pp. 243-248, 1999.

[17] I. Zagorodnov, "Ultra-short low charge operation at FLASH and the European XFEL", Proc. FEL'10, Malmö, Sweden.